Correction of detector noise and recalibration of NOAA/MEPED energetic proton fluxes

T. Asikainen,[1] K. Mursula,[1] and V. Maliniemi[1]

Received 3 February 2012; revised 13 July 2012; accepted 14 July 2012; published 6 September 2012.

[1] We report here on new problems in the NOAA/MEPED instruments and the related energetic proton dataset. These problems are solved, and the implied modifications to the earlier recalibration of the dataset are evaluated and adopted. We show that, besides degrading due to radiation damage, the NOAA-12 and NOAA-08 satellites suffer from increased electronic noise in the back detector of the proton instrument. We correct the effects of the noise, and present improved estimates for the effective energy thresholds of the MEPED proton detectors which are now determined more robustly than previously. We show that the cumulative Ap index can be used to produce a refined estimate for the temporal evolution of the effective MEPED energy thresholds. The derived energy thresholds of all MEPED instruments increase systematically with the cumulative particle fluxes, and this increase is similar in all satellites. Using the improved energy thresholds we obtain a uniform series of corrected MEPED energetic proton fluxes above 120 keV from 1979 onwards. We find that, due to the effect of the radiation damage and noise, the uncorrected fluxes at these energies were underestimated in the worst case by more than an order of magnitude, and that the earlier correction method also occasionally led to underestimation of the fluxes by nearly an order of magnitude. Such underestimation becomes severe already 1–2 years after the launch of the satellite.

Citation: Asikainen, T., K. Mursula, and V. Maliniemi (2012), Correction of detector noise and recalibration of NOAA/MEPED energetic proton fluxes, *J. Geophys. Res.*, *117*, A09204, doi:10.1029/2012JA017593.

1. Introduction

[2] One of the longest nearly continuous datasets of magnetospheric energetic particle measurements has been provided by the NOAA/POES (Polar Orbiting Environmental Satellites) satellite program which has been operational since 1978, i.e., already for three complete solar cycles. The dataset has been used extensively, e.g., in studying the particle precipitation in auroral zones [e.g., *Wissing et al.*, 2008; *Lam et al.*, 2010], constructing radiation belt models [e.g., *Fung*, 1996; *Huston et al.*, 1996], and studying magnetic storm dynamics [e.g., *Søraas et al.*, 2002, 2004; *Asikainen et al.*, 2005], the South Atlantic Anomaly [e.g., *Asikainen and Mursula*, 2005, 2008] and long-term variations in the radiation belts [e.g., *Fung et al.*, 2006; *Evans et al.*, 2007; *Rodger et al.*, 2010]. Accordingly, the NOAA/POES dataset has established itself as one of the most important and unique long-term energetic particle datasets in space physics.

[3] The energetic proton detectors measuring the directional fluxes of protons from 30 keV to 6.9 MeV have been shown to suffer from radiation damage that degrades the instruments by increasing the effective instrument energy thresholds. This leads to erroneous fluxes and artificial long-term trends in the data [*Galand and Evans*, 2000; *McFadden et al.*, 2007; *Asikainen and Mursula*, 2011]. We have recently conducted an extensive analysis of the entire NOAA/MEPED database and published the effective instrument energy thresholds and a method using these thresholds to correct the proton fluxes for the effects of radiation damage [*Asikainen and Mursula*, 2011] (hereinafter referred to as AM2011). The correction was shown to improve the overall continuity between the average proton flux levels of different satellites, which were found to differ by almost two orders of magnitude in the worst case before the correction. The correction of the proton fluxes had a significant effect especially on the long-term evolution of the fluxes. Although the electron detectors of MEPED do not suffer so much from radiation damage, the correction of proton fluxes affects also the electron data. This is because the electron detectors are sensitive to energetic protons at a certain energy range. It is possible to correct the effect of proton contamination in the electron data but this requires accurate knowledge of the proton fluxes.

[4] In this paper we will show that in addition to the radiation damage the NOAA-08 and NOAA-12 satellites suffer from an effect of electronic noise in the back detector chip which

[1]Department of Physics, Centre of Excellence in Research, University of Oulu, Oulu, Finland.

Corresponding author: T. Asikainen, Department of Physics, Centre of Excellence in Research, University of Oulu, PO Box 3000, FI-90014 Oulu, Finland. (timo.asikainen@oulu.fi)

0148-0227/12/2012JA017593

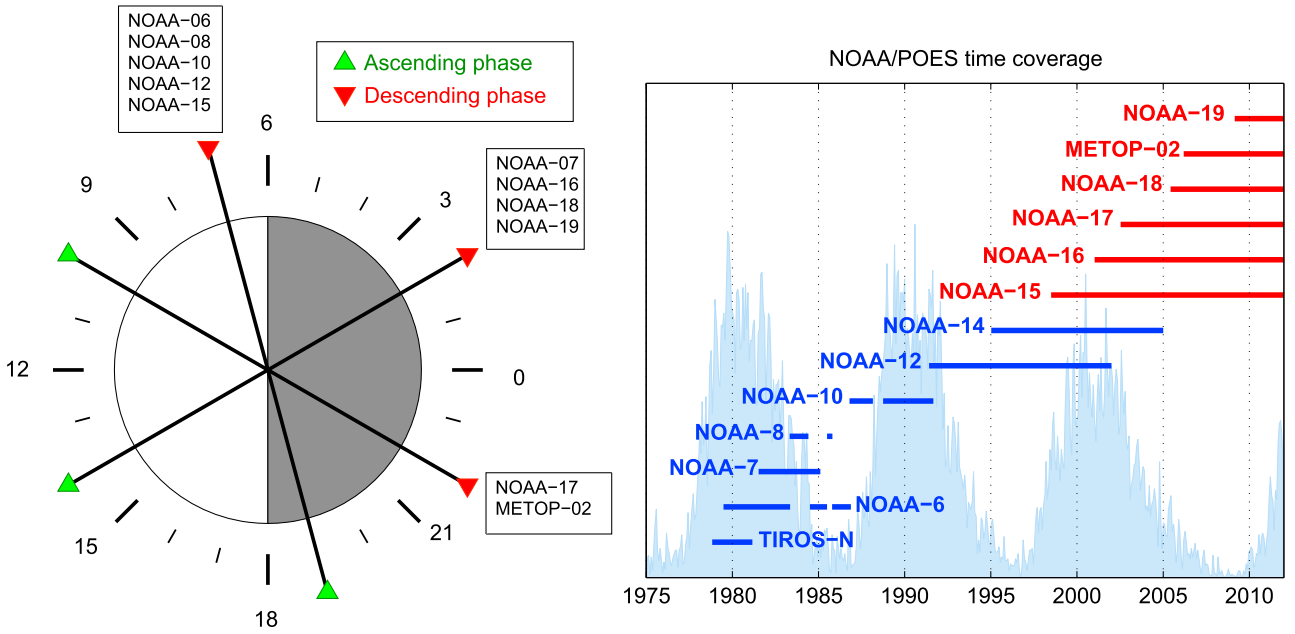

Figure 1. (left) Nominal orbital planes of the different NOAA satellites. The green upward (red downward) triangles depict the ascending (descending) phase of the satellite orbit and the tick marks depict MLT sectors. Note that from 2001 to 2005 NOAA-16 had an orbital plane similar to, e.g., NOAA-18 but after 2005 it started to rotate towards the dawn-dusk orbital plane like that of NOAA-15 which it reached by 2008. (right) The operational periods of all NOAA satellites with respect to the solar cycle.

significantly decreases the count rates of all energy channels measured by the front detector chip. Before correcting the effects of the radiation damage the detector noise problem must be corrected. Here we discuss this newly found problem in the data and present a method for correcting it. In addition we determine the effective energy thresholds of NOAA-06 and NOAA-12 more robustly than in AM2011 where the low number of satellite conjunctions resulted in poor statistics. We will also present improved methods of determining the temporal development of the energy thresholds for all satellites.

[5] The paper is organized as follows. Section 2 describes the basic properties of the NOAA satellites and the MEPED instrument including the effects of radiation damage. In Section 3 we discuss the problems caused by the increased electronic noise of the back detector in NOAA-08 and NOAA-12 and present methods for correcting them. In Section 4 we determine the energy thresholds of NOAA-06 and NOAA-12 more robustly than in AM2011 by using daily averaged fluxes. In Section 5 we show how the MEPED energy thresholds increase systematically with cumulative Ap index. Section 6 shows how we estimate the temporal evolution of the energy thresholds of the older satellites carrying a SEM-1 version of MEPED instrument with the cumulative Ap index. In Section 7 we discuss the relationship between the energy thresholds and the corrected cumulative proton fluxes. In Section 8 we discuss the additional refinements to the energy thresholds of the newer SEM-2 satellites and present the energy threshold factors in tabular format for all satellites as a function of time. In Section 9 we discuss the improvement in the time series of the proton fluxes obtained by the new correction methods presented here in comparison to those presented in AM2011. The conclusions are given in the last section.

2. NOAA/POES Satellites and the MEPED Instrument

[6] The NOAA/POES satellites fly around the Earth on nearly circular, polar orbits with a nominal altitude of about 850 km and an orbital period of about 102 min. The orbital planes relative to the Sun-Earth line stay relatively constant ("Sun synchronous") although over a period of several years the orientation of the orbital planes of some satellites rotates significantly (e.g., NOAA-16 orbital plane in 2001 was post-midnight-afternoon like NOAA-18, but in 2005 it started to rotate towards the dawn-dusk plane like that of NOAA-15 which was reached by 2008). The nominal orbital planes and operational periods of the different NOAA satellites are schematically shown in Figure 1.

[7] The NOAA satellites include a SEM (Space Environment Monitor) instrument package for measuring energetic protons and electrons. The satellites up to NOAA-14 had the SEM-1 version of the instrument package, while starting from NOAA-15 the satellites carry an improved version called SEM-2. The MEPED (Medium Energy Proton Electron Detector) instrument, which is a part of SEM, consists of two separate sub-instruments that measure energetic electrons and protons. We note that the data produced by the MEPED instrument onboard NOAA-14 is mostly unusable due to an unknown problem in the instrument operation and for that reason is not used in this work. Energetic electrons in MEPED are measured at nominal energy range above 30 keV in three integral energy channels, and energetic

Table 1. Nominal Energy Ranges of the MEPED SEM-2 Instrument[a]

Energy Channel	Nominal Energy Range of Protons (keV)	Nominal Energy Range of Contaminating Electrons (keV)
P1	30–80	-
P2	80–250	-
P3	250–800	-
P4	800–2500	-
P5	2500–6900	(≳800[b] for SEM-1)
P6	>6900 (no P6 in SEM-1)	≳800[b]
Energy Channel	**Nominal Energy Range of Electrons**	**Nominal Energy Range of Contaminating Protons**
E1	>30	210–2700 (135–1850 in SEM-1)
E2	>100	280–2700 (225–1850 in SEM-1)
E3	>300	440–2700 (430–1850 in SEM-1)

[a]The energy ranges for SEM-1 version of the instrument are the same except when indicated otherwise. The P-channels refer to proton detector and E-channels to electron detector. Both detectors are sensitive to both particle species to some degree. The proton counting efficiency of the electron channels is 100%.

[b]The nominal electron counting efficiency of P6 (SEM-2, P5 in SEM-1) channel is estimated by the instrument builder to be about 30% of incoming relativistic electrons. The sensitivity of P1-P3 channels to energetic electrons is negligibly small and P4-P5 (P4 in SEM-1) are not sensitive to electrons at all.

protons at nominal energy range from 30 keV upwards in six differential energy channels (the MEPED in SEM-1 package had only five differential proton channels). The nominal energy thresholds of the MEPED instrument are shown in Table 1. For a more detailed discussion of the instrument operation and configuration including a schematic of the instrument design we refer the reader to, e.g., *Seale and Bushnell* [1987] and *Yando et al.* [2011]. The protons and electrons are measured in two nearly orthogonal directions with a sampling time of 2 sec (the two directions are sampled on alternating seconds). In SEM-2 the local vertical telescope, the so called 0° telescope points away from the Earth along the radial Earth-satellite line (towards −X axis in satellite coordinates) and the local horizontal telescope, the so called 90° detector, points antiparallel to spacecraft velocity vector (towards +Y axis of the satellite coordinate system). To ensure a clear field of view the 0° telescope has been rotated by 9° from −X axis towards the −Z axis and the 90° telescope has been rotated by 9° from +Y towards −Z axis. (However, in METOP-02 the telescopes point directly towards −X and +Y axes respectively). This orientation of the telescopes means that at high latitudes where the magnetic field lines near the Earth are nearly radial the 0° telescope measures roughly field aligned precipitating particles and the 90° telescope measures roughly locally trapped particles. At low latitudes the situation is opposite so that the 90° telescope measures roughly field-aligned particles (either precipitating or upflowing, depending on the direction of satellite motion and the hemisphere) and 0° telescope locally trapped particles. However, we note that as the field of view of the telescopes is 30° the actual range of pitch angles that the telescopes see can be quite large. In SEM-1 the spacecraft coordinate system differs from that of the SEM-2 satellites. The SEM-1 X-axis points towards the Earth as in SEM-2 but the Y-axis points along the spacecraft velocity vector and Z-axis completes the right handed set. Accordingly the Y- and Z-axes in SEM-1 are opposite to those in SEM-2. In SEM-1 the 0° telescope is pointed precisely along the −X axis (no 9° tilt as in SEM-2). The 90° telescope, however, is pointed towards the −Z axis from where it has been rotated by 9° towards −X axis. Accordingly, the angle between the orientations of the 0° and 90° telescopes is 81° for SEM-1 and 88.6° for SEM-2. The measured count rates (particles/sec) are converted to physical fluxes (particles/cm^2 sr s) by dividing with the geometric factor G of the detector. For SEM-1 the geometric factor is $G = 0.0095$ cm^2 sr and for SEM-2 $G = 0.01$ cm^2 sr. A more detailed description of SEM-1 is given by *Hill et al.* [1985], *Seale and Bushnell* [1987], and *Raben et al.* [1995] and SEM-2 by *Evans and Greer* [2000].

[8] The MEPED proton detectors have been observed to degrade over time due to radiation damage, which has led to erroneous fluxes and artificial long-term trends in the data [*Galand and Evans*, 2000; *McFadden et al.*, 2007; *Asikainen and Mursula*, 2011]. In AM2011 we made a quantitative analysis of the effects of radiation damage on the MEPED proton detectors and presented a method for recalibrating the fluxes. We showed that the data in the beginning of the operational period of each satellite is fairly reliable but already after about 1–2 years the radiation damage has degraded the instruments so that the data can no longer be trusted without recalibration. The MEPED proton and electron instruments are based on solid state silicon detectors which are well known to suffer from radiation damage caused by the particles that are being measured [*Lutz*, 1999; *Grupen and Shwartz*, 2008]. The incoming particles affect the instruments by, e.g., creating various defects in the solid state silicon lattice. These defects can arise if an incoming particle, e.g., displaces one or several lattice atoms from its position (thus creating point or cluster defects and interstitial atoms which were dislocated from these sites) or if an energetic particle creates a large amount of space charge locally in some part of the lattice. These defects, among other things, reduce the mobility of free charge carriers. This affects the detection of incoming particles which is based on measuring the amount of free charge (proportional to the kinetic energy of particle) they release in the detector chip. This charge is collected by the instrument electronics within an integration time of 85 ns and converted to a voltage pulse whose amplitude is measured. The reduced mobility of the free charges reduces the amount of collected charge and thus leads to underestimation of particle energy. Thus in effect, the radiation damage increases the energy thresholds of the instrument from their initial nominal values. Since the measured fluxes typically decrease as a function of energy the radiation damage leads to underestimation of particle flux at a given energy channel. In AM2011 we estimated the factors by which energy thresholds of the three lowest proton energy channels have increased as a function of time for all the NOAA/POES satellites. In AM2011 and in this paper we refer to these factors as α factors. These α factors can be used to correct the fluxes. To do this we use here the same procedure as in AM2011 where we first fit in log-log scale a piecewise interpolating polynomial to the measured integral spectrum taking into account that the energy thresholds have increased by the α factors. By taking the difference of the

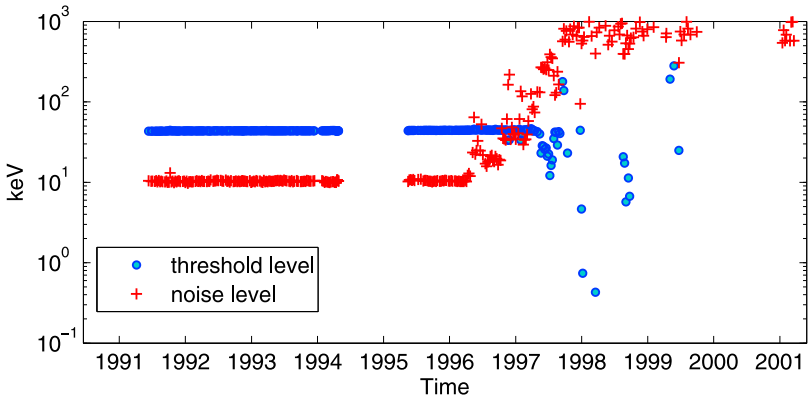

Figure 2. Electronic channel threshold (blue points) and noise level (red crosses) for the back detector (channel P5) of NOAA-12 0° telescope.

integral flux at two different energies the interpolating polynomial allows us to compute the fluxes at any desired energy range although the goal of the correction is to compute the fluxes at the nominal instrument energy thresholds. However, as discussed in AM2011, computing the flux at any energy which is below the lowest energy measured by the instrument (defined by P1 α factor) is problematic because one has to extrapolate the interpolating polynomial. This was shown to cause significant overestimation of the flux even when the α factors are still small. Accordingly, the highest value of the P1 α factor during a satellite's operational period essentially determines the lowest energy above which we always get reliable estimates for the flux. When comparing several satellites it is the highest value of P1 α factors of all satellites that determines the lowest usable energy threshold.

3. Correcting the Back Detector Noise in NOAA-12 and NOAA-08

[9] Both 0° and 90° telescopes contain two separate detector chips, the front and the back detector. In SEM-1 the front detector measures energy channels P1-P4 and the back detector measures those high energy protons which penetrate through the front detector and deposit energy also into the back detector. These counts are recorded in the 5th energy channel P5. The front and back detectors operate in anti-coincidence so that if a count is registered in the back detector it is not recorded in the channels of the front detector. The MEPED instruments have been regularly running onboard in-flight calibrations to monitor the electronic energy thresholds of the separate energy channels and also the noise levels for these thresholds. These calibrations are based on feeding controlled voltage pulses, simulating incoming particles, to the MEPED counting electronics and observing the response. By fitting a gaussian to the response as a function of pulse amplitude, we can obtain the threshold level and the width of the gaussian (noise level). The procedure for analyzing the in-flight calibration data is discussed by *Seale and Bushnell* [1987]. Note that the monitored electronic threshold is not the same as the effective instrument energy threshold which is subject to radiation damage. The electronic thresholds describe the channel thresholds in the pulse height analyzer and are not sensitive to the effects of radiation damage to the detector chip. Figure 2 (courtesy of R. Bushnell and D. Evans NOAA Space Environment Center) shows the electronic energy threshold (blue points) and corresponding noise level (red crosses) in equivalent particle energy (keV) for the back detector of the NOAA-12 0° telescope. One can see that the threshold and the noise level stay quite constant until May 1996. (Note that there is a gap in these measurements in 1994–1995). After May 1996 the noise level dramatically increases and reaches a new constant level around 500–1000 keV in 1998. Somewhat later in 1997 the back detector threshold level also starts to show anomalous behavior. In effect, since 1997 the energy threshold of the 0° back detector is very poorly defined due to increased electronic noise and this leads to increased noise counts recorded by the back detector. (Note that the electronics of the 90° back detector did not suffer from noise.) The increase in the back detector count rate is seen in Figure 3a which shows the daily averaged flux of the 0° P5 channel of NOAA-12 as a function of time. In order to avoid the effects of the South Atlantic Anomaly (e.g., contamination by intense relativistic electron fluxes) the daily averages were computed using only the data from the northern hemisphere above $L = 2$. One can clearly see how the base line of back detector fluxes increases in 1997 to a new level, about 6 times higher.

[10] The noise in the back detector also affects the counts in the lower energy channels recorded by the front detector. This is due to the anti-coincident logic between the two detectors, which erases a count from the front detector when a count appears in the back detector. Thus, increased noise count level in the back detector decreases the count rates of the front detector by a certain factor. Figure 3b depicts the ratio of daily averaged 0° and 90° P1 fluxes from NOAA-12. Figure 3b shows that the ratio of uncorrected 0° and 90° P1 fluxes steadily increases in time up to 1997 due to the radiation damage which degrades the 90° detector faster than the 0° detector. In 1997, concurrently with the increase in the 0° back detector noise levels, there is a sharp decrease in the 0° P1/90° P1 ratio indicating that the 0° fluxes decrease rapidly relative to the 90° fluxes. In 1998 the ratio sets to a new, lower level and stays relatively steady afterwards. A similar behavior of the 0° fluxes is also visible in P2,

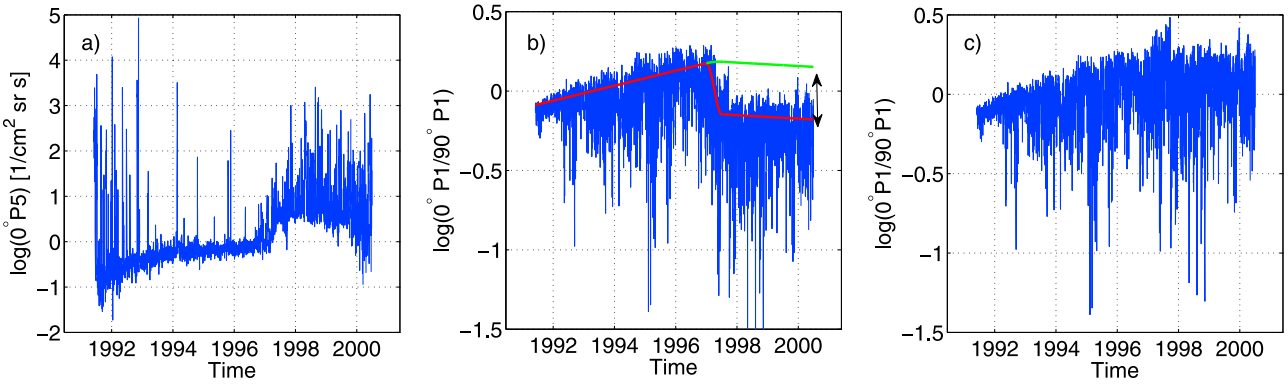

Figure 3. (a) Daily averaged fluxes of NOAA-12 0° P5 channel. (b) Logarithmic ratio of the daily averaged, uncorrected 0° and 90° P1 fluxes. The red lines depict fitted trends in the ratio and the green curve shows the new, proper trend for the ratio. (c) Logarithmic ratio of the daily averaged, uncorrected 0° and 90° P1 fluxes after correction for back detector noise.

P3 and P4 energy channels (not shown here). We note that not all the counts observed in the P5 channel are due to noise. The effect of the noise is to increase the average level of the background counts. Accordingly, the evolution of the noise can be best determined by examining the quiet time baselines of the fluxes and flux ratios.

[11] To correct the artificial decrease in the 0° channels due to the back detector noise we determined the linear trends for the baseline of the logarithmic ratio for the time periods before 1 January 1997 (period 1) and after 2 July 1997 (period 3). The trends were determined by fitting a line to the local maxima of the logarithmic 0°/90° flux ratio. The local maxima were defined as those points which have a larger value than the two surrounding points. These linear fits are shown in Figure 3b. Then we determined the trend for the period between 1 January 1997 and 2 July 1997 (period 2) by computing a 3rd order polynomial which continuously connects to the linear trends of periods 1 and 3 and whose derivative at the end points matches the slopes of the linear trends of periods 1 and 3. This polynomial trend is also shown as a part of the red curve in Figure 3b. We then subtracted from period 2 the polynomial trend and determined a new correct trend for period 2 by requiring that the slope of this trend changes linearly from the slope of period 1 to the slope of period 3 over the period 2 and is continuous with the trend of period 1. With these boundary conditions we obtained a 2nd order polynomial trend. Finally the logarithmic 0°/90° ratio of period 3 was increased by an offset determined by the difference between the new trend of period 2 and the linear trend of period 3 at the crossover point (see the arrow in Figure 3b). The resulting new trend after period 1 is shown by the green curve in Figure 3b. The result of these operations is shown in Figure 3c. One can see that these corrections remove the abrupt decrease in the ratio and raise the ratio to the correct level in period 3. We note that the corrected ratio in Figure 3c resembles quite well the overall temporal evolution of the 0°/90° ratios in the other satellites which do not suffer from the noise problem. Typically the 0°/90° ratio increases in time because the 90° telescope is usually subjected to larger degrading fluxes than the 0° telescope [*Galand and Evans*, 2000]. Since the 90° detector does not suffer from the noise problem the correction is made by applying the above operations to the logarithmic 0° fluxes of P1 and P2. For P3 and P4 channels the sudden decrease in the count rate baseline is better seen in the 0° count rates separately instead of 0°/90° flux ratio. Because of this, the noise correction in the P3 and P4 channels was done by fitting the baseline trends to the 0° count rates directly. The increase in the back detector fluxes in the 0° P5 channel was corrected with the same operations to logarithmic 0° P5 fluxes.

[12] NOAA-08 was launched in May 1983 and produced measurements for about a year until June 1984 when the MEPED instrument was temporarily turned off. In 1985 the MEPED of NOAA-08 was operating again for about three months in July-October. Near the end of its operational period, starting from 1 August 1985, the back detector noise in the 90° telescope of NOAA-08 suddenly increased similarly as in the 0° telescope of NOAA-12 in 1996. In the case of NOAA-08 the electronic noise increase was so severe that the detector response to in-flight calibration pulses was completely erratic and the in-flight calibrations could not be reliably used to estimate the electronic threshold levels anymore. The increase in the 90° back detector noise level is seen as an increased flux level in the 90° P5 channel depicted in Figure 4a. As in NOAA-12 the noise in the back detector decreased the count rates in the channels of the front detector. This led to a sharp increase in the 0°/90° proton ratio as depicted for the P1 channel in Figure 4b. Note that the ratio just before the increase is slightly smaller than before the data gap in 1984. This is due to natural variations in the 0°/90° ratio that are also present in NOAA-12, e.g., in 1995 (Figure 3b). Note also that the depicted time interval for NOAA-08 in Figure 4 is considerably shorter than that for NOAA-12 in Figure 3.

[13] To correct the 90° telescope data starting from 1 Aug 1985 for the effect of the increased back detector noise we used a similar method as for NOAA-12. However, the noisy time period and the noiseless time period determining the correct level of the 0°/90° ratio are now relatively short. Due to the large variations naturally present in the 0°/90° ratio, we cannot reliably determine linear fits to the data. Instead, we have determined the base line level of the period from 1 July 1985 to 31 July 1985 (period 1) and the period starting from

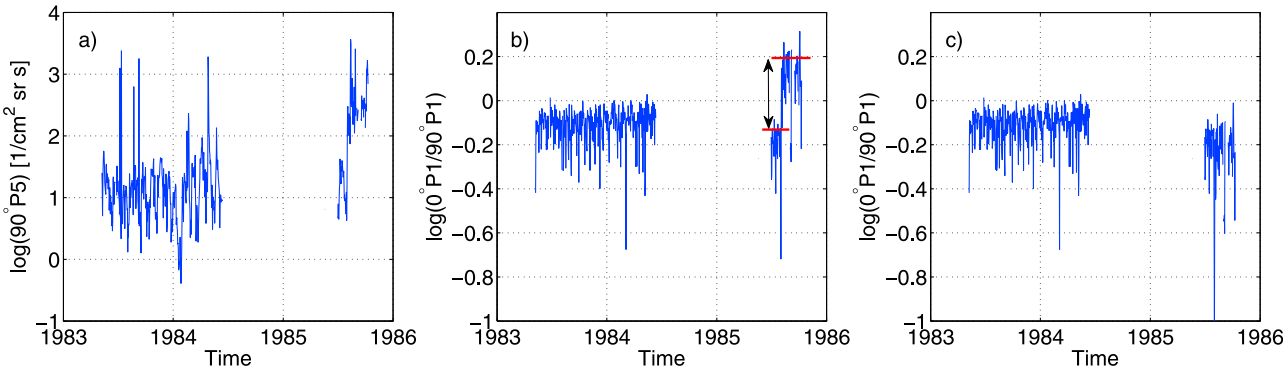

Figure 4. a) Daily averaged fluxes of NOAA-08 90° P5 channel. b) Daily averaged logarithmic ratio of 0° and 90° P1 fluxes. The red lines depict the baseline levels in the ratio. c) Daily averaged logarithmic ratio of 0° and 90° P1 fluxes after correction for increased back detector noise.

1 August 1985 (period 2) by computing the median of the local maxima in the logarithmic ratio for the two periods. The 90° flux was then scaled up by a factor determined by the difference between the base line levels in logarithmic scale. The corrected 0°/90° ratio of P1 channel is shown in Figure 4c. As for NOAA-12 the noise correction was made for all energy channels.

4. Revised α Factors for NOAA-06 and NOAA-12

4.1. NOAA-06

[14] The temporal evolution of the α factors in the SEM-1 satellites is more uncertain than in the SEM-2 satellites. This is because before 1998 satellites were launched very sparsely in time and the periods of simultaneous measurements by a new and an old satellite were short. Fortunately all SEM-1 satellites (NOAA-06, NOAA-08, NOAA-10 and NOAA-12) except NOAA-07 were on the same orbit, although the orbital phasings were different. In AM2011 the α factors for these satellites were determined by using exact satellite conjunctions which occurred seldom and led to poor statistical significance of the estimated α factors. To obtain more robust estimates for the energy thresholds of the NOAA-06 satellite we used here the daily averaged fluxes (and integral spectra) to determine the α factors. The daily averages were computed from measurements obtained from the northern hemisphere at $L > 2$. The daily averaged spectra of NOAA-06 were compared with the simultaneous daily averaged spectra from NOAA-10 in October 1986 after the launch of NOAA-10. The α factors were determined using the same spectral comparison methods as in AM2011, essentially by determining how much the energy thresholds of the old satellite must be increased for the fluxes to match those of the new satellite. Even though these satellites do not sample the same MLT sector at exactly the same time (the largest time difference being roughly 50 min) the average flux levels can be expected to be roughly equal over time scales of several days to months because of the same orbital plane. In AM2011 the α factors of NOAA-06 were linearly extrapolated in time using only one α factor determined in 1981–1982 using exact satellite conjunctions after the launch of NOAA-07. The additional α factors determined here for NOAA-06 using daily averages allow us to better estimate the temporal evolution of the α factors for the whole duration of the NOAA-06 measurements. Figure 5 shows the revised NOAA-06 α-factors for 0° (blue

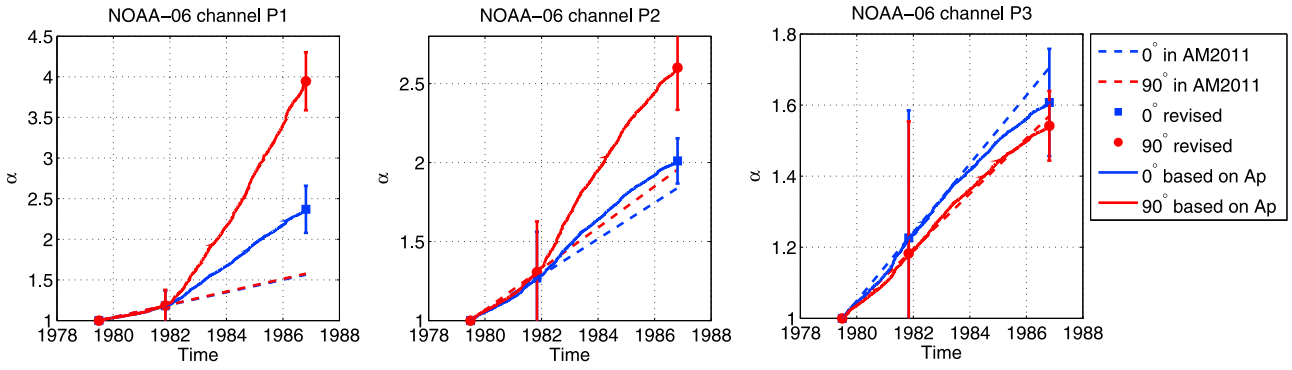

Figure 5. Revised α factors for the three lowest proton energy channels of NOAA-06 which were obtained by exact conjunctions between NOAA-07 (in 1981) and by comparing the daily fluxes of NOAA-06 to simultaneous fluxes of NOAA-10 (in 1986). The red circles depict the 90° telescope and the blue squares the 0° telescope. The dashed lines represent the temporal evolution of the α factors as determined in AM2011. The solid curves depict the temporal evolution of the revised α factors based on cumulative Ap index.

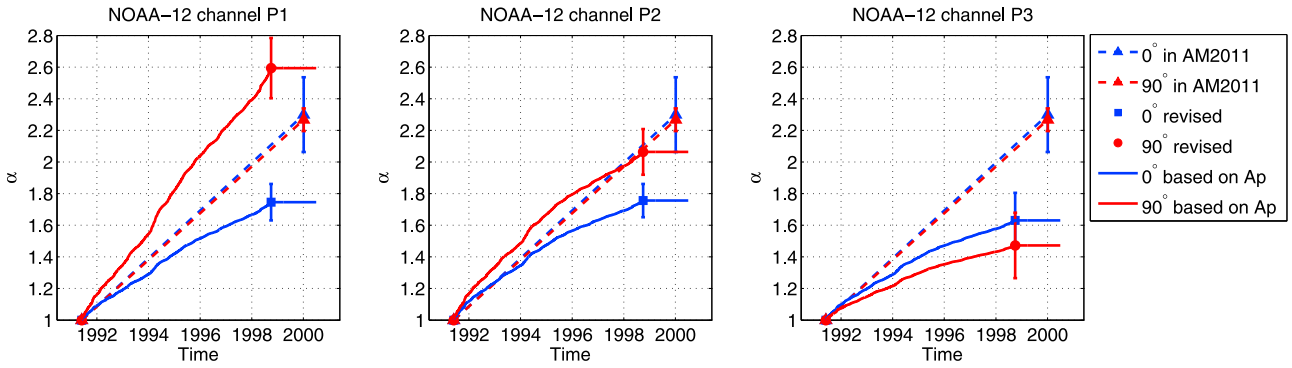

Figure 6. Revised α factors for the three lowest proton energy channels of NOAA-12 which were obtained by comparing the daily fluxes of NOAA-12 to simultaneous fluxes of NOAA-15 in 1998. The red circles depict the 90° telescope and the blue squares the 0° telescope. The dashed lines and triangles represent the temporal evolution of the α factors as determined in AM2011. The solid curves depict the temporal evolution of the revised α factors (determined after NOAA-12 noise correction) based on cumulative Ap index.

squares) and 90° (red circles) telescopes. One can see that the linear extrapolation (dashed lines in Figure 5) between the first two points used in AM2011 would lead to a severe underestimation of the α-factors especially in the two lowest energy channels. The solid curves depict the estimated temporal evolution of the α factors based on cumulative Ap index. The relation between the α factors and the cumulative Ap index and its use for estimating the temporal evolution of the α factors will be discussed below in Sections 5 and 6.

4.2. NOAA-12

[15] After the correction of the back detector noise in NOAA-12 0° telescope we determined the new α factors for NOAA-12 by comparing the daily averaged integral spectra of NOAA-12 and NOAA-15 from 1 July 1998 to the end of 1998. The 0° telescopes in NOAA-12 and NOAA-15 point roughly in the same direction and thus can be compared with good confidence but the 90° telescopes in the two satellites are roughly perpendicular to each other (because of the change in SEM configuration; see Section 2) so that the data of the two satellites from these telescopes can not be compared directly. However, if the data is taken from a region where the fluxes in these two directions (90° directions in NOAA-12 and NOAA-15) can be assumed to be equal the measurements from the 90° detectors can be compared with good confidence. During quiet times the isotropic boundary (the latitude above which energetic particle fluxes are isotropic) at local midnight is close to 65° invariant latitude, i.e., roughly at L = 6 [*Asikainen et al.*, 2010]. During disturbed times the isotropic boundary moves to lower latitudes. Accordingly, we can expect the fluxes to be always roughly isotropic above L = 6. Using this result, we computed for NOAA-12 and NOAA-15 the daily averages using data only above L = 6 and then determined the 90° α factors using this limited dataset. Figure 6 shows the NOAA-12 α factors for the three lowest energy channels. Each panel shows the new revised α factors for the 0° (blue) and 90° (red) telescopes. The blue squares and red circles depict the new α factors obtained using daily averages after noise correction and the triangles with dashed lines depict the old α factors and their corresponding temporal evolution determined originally in AM2011. The solid curves depict the temporal evolution of the revised α factors based on cumulative Ap index which will be discussed in detail below (Sections 5 and 6). One can see that the new factors differ from the old ones. Especially the α factors of the 0° telescope have decreased relative to the 90° α factors in P1 and P2 channels. Previously, the noise problem decreased the 0° fluxes too low and resulted in excessively large α factors. The number of NOAA-12/NOAA-15 conjunctions used in AM2011 was very low due to opposite orbital phasing, and resulted in poor statistics. The new method of using daily averages is more robust and permits us to estimate the α factors for P2 and P3 channels too. This was not possible in AM2011 due to low statistics in these channels whence the same α factors for all energy channels were used there.

5. Dependence of the α Factors on the Cumulative Ap Index

[16] Geomagnetic activity indices like the Ap index can be used as a crude proxy for the intensity of the magnetospheric energetic particle fluxes. Accordingly, the total particle fluxes degrading the instruments should be roughly proportional to the cumulative Ap index. Figures 7 and 8 show the relationship between the 90° and 0° α factors and the cumulative daily Ap indices defined as

$$C_{A_p}(n) = \sum_{i=1}^{n} \mathrm{Ap}(i), \tag{1}$$

where $i = 1$ corresponds to the first day of the corresponding satellite. The plots show only the comparable satellites on similar dawn-dusk orbit (NOAA-06, NOAA-10, NOAA-12 and NOAA-15). The solid lines in the plots depict linear fits with a constant offset of one to all the data points. One can see a clear relation between the C_{A_p} and the α factors. In the P1 channels we found that the best fit to the points is obtained if the α factors are plotted on a logarithmic scale. In the 90° P1 channel the only point that deviates from the fit with the cumulative Ap is the last α factor of NOAA-06 ($\alpha \approx 4$). However, when the α factors are viewed with respect

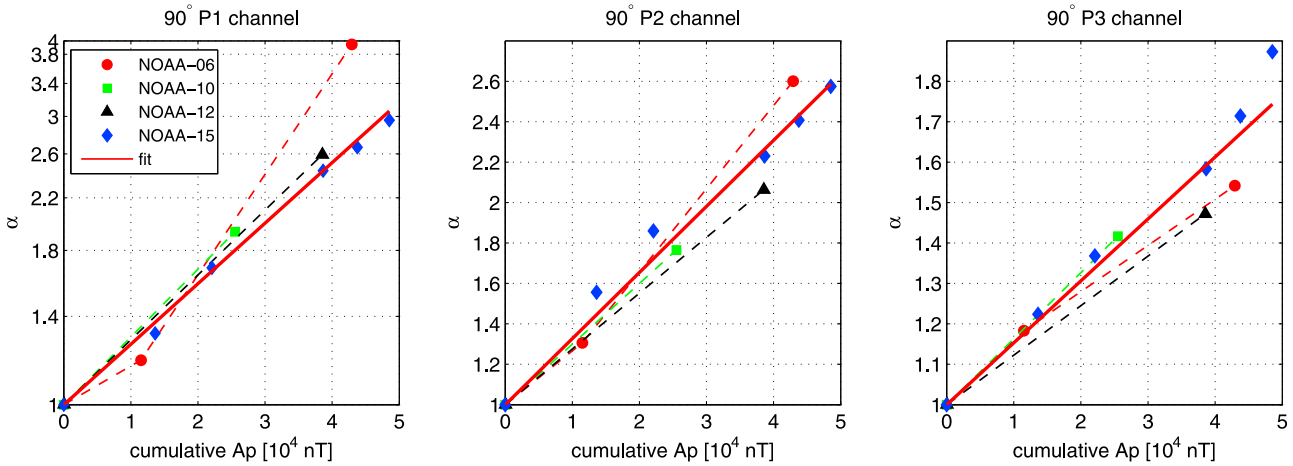

Figure 7. The relationship between 90° detector α factors and cumulative daily Ap index for all the satellites on similar dawn-dusk orbit. The solid lines in the plots depict linear fits with a constant offset of 1 to the data. The dashed lines show the piecewise linear fits to the α factors of individual satellites. Energy channels (left) P1, (middle) P2, and (right) P3. Note the logarithmic spacing for the P1 channel.

to the cumulative corrected proton fluxes, the same NOAA-06 point is not an outlier (see Figure 10 below and corresponding discussion in Section 7). This indicates that the Ap index cannot entirely represent the intensity of the degrading particle fluxes. This is particularly true during intense storms where the Ap activity can be relatively short lived compared to the long lifetime of intense energetic particle populations created deep in the inner magnetosphere. It should be noted that the NOAA-06 time period contains very intense storms in mid-1982 and in February 1986, which was one of the largest storms of the last three decades. Intense events like these create long lasting particle populations that degrade the NOAA-06 instruments well after Ap activity has subsided. The slopes of the fits (between $\log(\alpha)$ and C_{Ap}) for the 90° and 0° P1 channels are $(0.231 \pm 0.010) \times 10^{-4}$ and $(0.175 \pm 0.015) \times 10^{-4}$ respectively indicating the fact that the 90° P1 channel degrades faster as a function of cumulative Ap than the 0° P1 channel. This is because the proton fluxes in the 90° channel are typically larger than in the 0° channel.

[17] For the P2 and P3 channels we found that a linear fit well describes the relation between the α factors and the cumulative Ap index. The slopes of the linear fits (between α and C_{Ap}) for the 90° and 0° P2 channels are $(0.33 \pm 0.02) \times 10^{-4}$ and $(0.245 \pm 0.015) \times 10^{-4}$ respectively. The slopes for the 90° and 0° P3 channels are $(0.153 \pm 0.013) \times 10^{-4}$ and $(0.167 \pm 0.013) \times 10^{-4}$ respectively. One can see that the P2 90° channels also degrade slightly faster as a function of cumulative Ap than the 0° channels. However, there is no statistically significant difference in the rate of degradation between the P3 90° and 0° telescopes. The rate of degradation decreases with energy channel so that the lower energy channels degrade faster.

[18] This inverse energy dependence of the rate of degradation is probably due to the fact that protons of different energies penetrate to different depths in the detector. Thus, the radiation damage caused by higher energy protons is localized deeper in the detector chip than the damage caused by lower energy protons. Accordingly, the radiation damage of the lower energy channels depends more on the lower

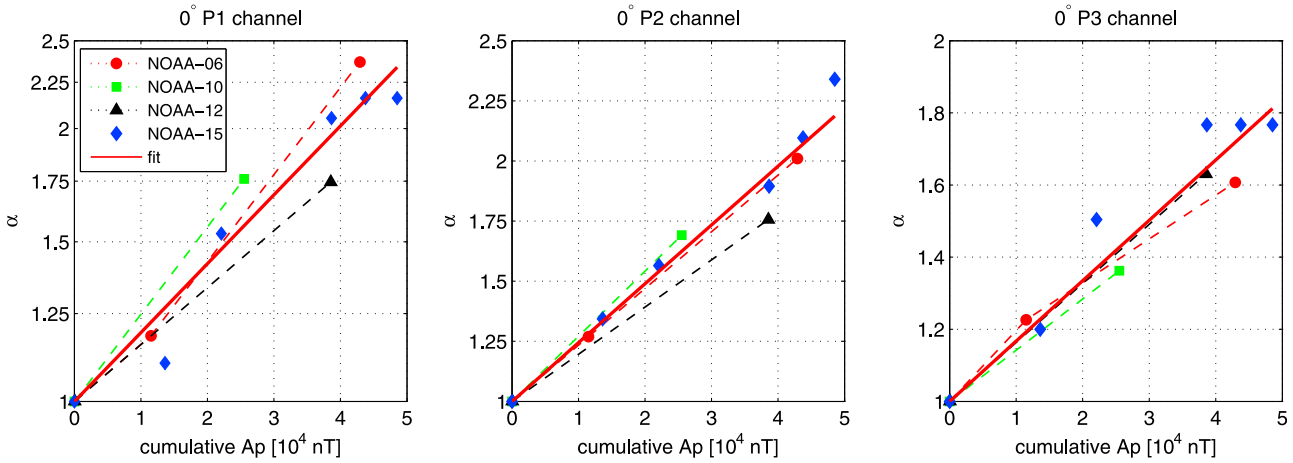

Figure 8. The same for the 0° detector as in Figure 7 for the 90°.

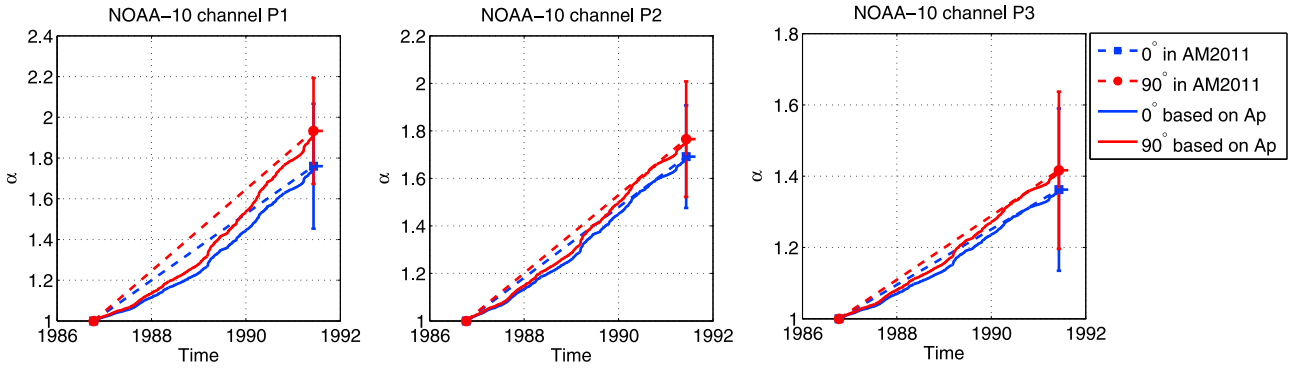

Figure 9. The α factors for the three lowest proton energy channels of NOAA-10. The red circles depict the 90° telescope and the blue squares the 0° telescope. The dashed lines represent the temporal evolution of the α factors as determined in AM2011. The solid curves depict the temporal evolution of the revised α factors based on cumulative Ap index.

energy proton fluxes while for higher energy channels the damage depends more on the high energy proton fluxes. Since typically the proton fluxes decrease strongly with energy the total damage caused by the higher energy protons is expected to be smaller than that of the lower energy protons, i.e., the radiation damage proceeds slower in the higher energy channels.

6. Temporal Evolution of SEM-1 α Factors

[19] In AM2011 we were able to determine only two α factors for each SEM-1 satellite. We then linearly interpolated between these two α factors to obtain the temporal evolution of the α factors for each SEM-1 satellite. However, the complicated nonlinear temporal evolution of the α factors of the SEM-2 satellites (for which several α factors could be determined) suggests that the temporal evolution of the α factors also in the SEM-1 satellites is generally nonlinear. Above we found that the α factors of NOAA-06, NOAA-10, NOAA-12 and NOAA-15 display a good correlation with the cumulative Ap index. This allows us to estimate the temporal evolution of α factors in the SEM-1 satellites (NOAA-06, NOAA-10 and NOAA-12) by computing the cumulative Ap index for each satellite and using the relation between the α factors and the cumulative Ap to determine the α factors at any given time. Instead of using the average linear fit (solid line in Figures 7 and 8) we use the piecewise linear trends of each satellite separately (dashed lines in Figures 7 and 8) in order to adjust the lines to the determined α factors. The temporal evolution of the α factors derived in AM2011 and the newly obtained α factors for NOAA-06 and NOAA-12 are shown in Figures 5 and 6 and for NOAA-10 in Figure 9. The α factors for NOAA-10 have remained the same as in AM2011 since a statistically significant number of direct satellite conjunctions were found for NOAA-10 and NOAA-12 in 1991. However, we also determined the NOAA-10 α factors in 1991 by using the daily averaged spectra, similarly as for NOAA-06 and NOAA-12 above, and found that the results were the same as in AM2011, within error limits. This corroborates that the two different methods of determining the α factors produce comparable results. In Figures 5, 6, and 9 the solid curves depict the time evolution of the α factors based on the cumulative Ap index. In each case the temporal evolution is significantly nonlinear. The time evolution of the α factors could similarly be estimated for the SEM-2 satellites, but this is not necessary since the SEM-2 satellites have α factors determined with a spacing of at most a couple of years. This is good enough to obtain a sufficiently accurate temporal evolution by interpolation and fitting with respect to time as done in AM2011. We have checked that for SEM-2 satellites the interpolation methods used in AM2011 produce very similar α factor temporal evolution as interpolation based on cumulative Ap.

7. The Relationship Between the α Factors and the Corrected Fluxes

[20] Typically, the effective energy thresholds in all NOAA satellites increase roughly by 30–50% during the first three years of operation depending on the energy channel and on the intensity of the radiation environment (AM2011). Since the radiation damage is caused by energetic particles it is reasonable to assume that the α factors in different satellites behave fairly similarly as a function of the cumulative radiation dose subjected to the instrument. To show whether this is true Figures 10 and 11 depict the α factors of 90° and 0° MEPED sensors from all satellites (except NOAA-07, NOAA-08 and NOAA-19) as a function of the corrected cumulative fluxes above 120 keV or 800 keV threshold energy. The cumulative fluxes were computed from daily averages that include all available data (in contrast to above where the daily averages contained only data from the northern hemisphere above L = 2). The energy limit of 120 keV in the case of P1 and P2 channels is defined by the maximum value of 90° P1 α factor in NOAA-06 (see Figure 5) which is the largest of all satellites and thus determines the lowest energy, i.e., 4 × 30 keV = 120 keV, above which we have a continuous series of measurements (see the discussion at the end of Section 2 on correcting the fluxes). As the main feature Figures 10 and 11 show a clear linear relation between the cumulative fluxes and the logarithmic α factors which is indicated by the fitted red lines in each energy channel. There is no systematic difference in this relation between the SEM-1 and SEM-2 telescopes. Comparing the α factors to the cumulative fluxes we have

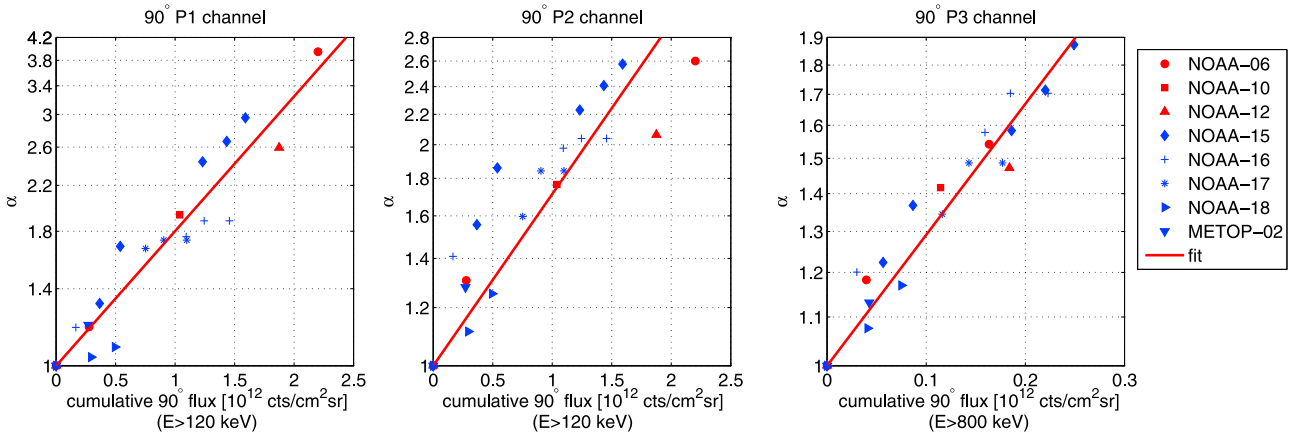

Figure 10. The relationship between 90° detector α factors and the corrected cumulative flux (above 120 keV for P1 and P2 and above 800 keV for P3) for different satellites in energy channels (left) P1, (middle) P2, and (right) P3. The vertical axis is logarithmic but the labels correspond to linear α values. The SEM-1 satellites are depicted with red symbols and the SEM-2 satellites with blue symbols.

found that the P1 and P2 channels show a good correspondence with cumulative fluxes above 120 keV energy while the P3 channels show a better correspondence with fluxes above 800 keV. The slopes of the fitted lines in Figure 10 for the 90° P1, P2 and P3 channels are $(0.59 \pm 0.03) \times 10^{-12}$, $(0.54 \pm 0.03) \times 10^{-12}$ and $(2.56 \pm 0.07) \times 10^{-12}$ respectively, and in Figure 11 for the 0° P1, P2 and P3 channels $(0.93 \pm 0.05) \times 10^{-12}$, $(0.96 \pm 0.04) \times 10^{-12}$ and $(4.5 \pm 0.3) \times 10^{-12}$ respectively.

[21] Comparing the P1 and P2 channels in both telescopes shows that the α factors degrade very similarly in both energy channels relative to the cumulative flux above 120 keV. The P3 channel is not directly comparable with P1 and P2 channels because of the different energy limits chosen for the cumulative flux. Comparing the degradation rate in 0° and 90° seems to suggest that the 0° detectors degrade faster than the 90° detectors, which does not agree with previous finding of faster degradation in 90° detectors. The discrepancy is most likely due to the fact that the energy limits chosen for the cumulative flux in Figures 11 and 10 do not correspond to the real energy range of the particle inflicting damage on the different energy channels. In fact, it is likely that most of the damage to the detectors is caused by the particles below 120 keV which have been neglected here because of the constraints imposed by NOAA-06. The degree to which the fluxes above 120 keV reflect the fluxes below 120 keV depends on the energy spectrum of the protons. The harder the spectrum (smaller spectral index) below 120 keV the smaller the ratio between cumulative fluxes above 120 keV and above 30 keV (lower limit of the instrument). If the spectrum in 90° telescope is harder on average than in 0° telescope the rates of degradation would be smaller in the 90° telescope. In fact, using still undegraded data from the beginning of a few satellites' time series, we have checked that the 90° spectra are typically somewhat harder than the 0° spectra. This suggests that the difference between the real degradation rates is significantly smaller than the apparent degradation rates depicted in Figures 11 and 10.

8. Revisions to α Factors in SEM-2 Satellites

[22] We showed in AM2011 that correcting the fluxes by the obtained α factors greatly improves the correspondence of fluxes between satellites on similar orbits. However, thereafter we noted that the fits obtained in AM2011, which

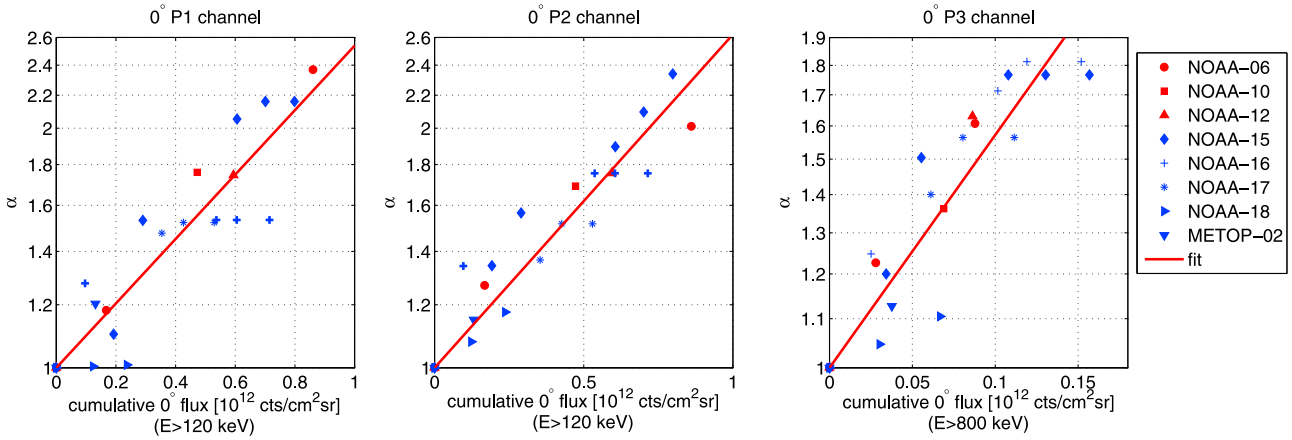

Figure 11. The same for the 0° detector as in Figure 10 for the 90°.

Table 2. Tabulated α-Factors for the 0° Proton Telescope of NOAA-06, NOAA-10 and NOAA-12 for Mid Point (2 July) of Each Year[a]

Year	NOAA-06	NOAA-10	NOAA-12
1980	1.06, 1.10, 1.08		
1981	1.14, 1.22, 1.18		
1982	1.30, 1.37, 1.28		
1983	1.57, 1.57, 1.38		
1984	1.80, 1.72, 1.46		
1985	2.06, 1.86, 1.53		
1986	2.30, 1.98, 1.59		
1987		1.05, 1.06, 1.03	
1988		1.18, 1.20, 1.10	
1989		1.35, 1.37, 1.19	
1990		1.57, 1.55, 1.29	
1991		1.76, 1.69, 1.36	1.02, 1.03, 1.02
1992			1.14, 1.18, 1.15
1993			1.25, 1.30, 1.25
1994			1.37, 1.43, 1.36
1995			1.47, 1.53, 1.44
1996			1.55, 1.60, 1.50
1997			1.63, 1.66, 1.55
1998			1.71, 1.73, 1.61
1999			1.75, 1.76, 1.63
2000			1.75, 1.76, 1.63

[a]Each column contains the α-factors for the three lowest energy channels respectively (α_1, α_2, α_3). Note that at the launch of a satellite the α-factors are 1.0 for the given satellite.

describe the temporal evolution of the α factors, in some cases produced systematic differences in the P3 90°/0° flux ratio between the SEM-2 satellites on comparable orbits. This is because in the P3 channels the low statistics in determining the α factors resulted in large uncertainties in the form of the fits. This problem was significant only in NOAA-15 0° P3 and METOP-02 0° P3 channels. We note that for the SEM-1 satellites the α factors and their temporal evolution determined above lead to consistent flux levels and 90°/0° flux ratio.

[23] For NOAA-15 and METOP-02 we have now slightly changed the form of the α fits (the fit is still well within the error limits of individual α factors) so that a better correspondence between NOAA-17 and METOP-02 and NOAA-15 and NOAA-16 after 2008 (see Figure 1 and note the change in NOAA-16 orbital plane) was obtained also in the 90°/0° flux ratio. In the comparison of SEM-2 satellites we used corrected (with α factors determined in AM2011) daily averaged fluxes computed from measurements from the northern hemisphere at L > 2. For NOAA-15 we found that a better result in the P3 channels is obtained by using separate fits for the 0° and 90° channels, which more closely follow the individual α factors, instead of using the same linear fit for both telescopes as was previously done in AM2011. In the METOP-02 satellite the temporal evolution of α factors is based on linear interpolation between two determined α factors. In 2009 the uncertainty in the 0° P3 α factor is quite large (40%) and thus makes the slope of the linear fit at P3 channel rather uncertain. In the 90° P3 channel the uncertainty of the α factor at 2009 is much smaller (16%). When we compared METOP-02 with NOAA-17 we found that the 90°/0° flux ratio was systematically lower in METOP-02 than in NOAA-17, and that a slightly better agreement between the two satellites was seen in the 90° P3 fluxes than in the 0° fluxes. These facts indicated that the temporal evolution of the 0° P3 α factor in METOP-02 was erroneous and needed adjusting. To improve the situation we have found that decreasing the slope of the linear fit of this α factor by 20% results in a better match in the 90°/0° flux ratio. This adjustment also produced better matching flux levels in the 0° P3 channels of METOP-02 and NOAA-17.

[24] In the process of checking the α factors of all SEM-2 satellites we also found that a couple of α factors for NOAA-17 and NOAA-18 satellites were slightly erroneously determined in AM2011. These errors were corrected, although the new fits for these corrected α factors are still well within the error limits of the α factors determined in AM2011. The α factors for the three lowest energy channels of the 0° and 90° telescopes for the SEM-1 (SEM-2) satellites have been shown in Tables 2 and 3 (Tables 4 and 5). The α factors shown in the tables have been calculated from the fits for the mid point (2 July) of each year as a set of three values corresponding to channels P1, P2 and P3.

9. Comparing the Corrected and Uncorrected Fluxes

[25] Let us now study the overall characteristics of the corrected (both the present revised correction and the correction in AM2011) and uncorrected energetic proton fluxes. As above, when determining the SEM-1 α factors, we have used here the daily averaged fluxes calculated from the northern hemisphere ($L > 2$) for the energy range 120–250 keV separately for the 90° and 0° telescopes. The daily averages were calculated over all satellites and local time sectors. We have, however, excluded here the NOAA-12 data after the NOAA-15 launch in 1 July 1998 because of the sparsity of the data.

[26] Figure 12 shows an overview of NOAA/MEPED energetic proton measurements in 1979–2011. The panels show the 30-day averages of 120–250 keV protons from the 90° and 0° telescopes. Note that there is a 7 month data gap

Table 3. Same as Table 2 but for the 90° Telescopes

Year	NOAA-06	NOAA-10	NOAA-12
1980	1.06, 1.11, 1.07		
1981	1.15, 1.25, 1.15		
1982	1.41, 1.49, 1.23		
1983	1.93, 1.83, 1.33		
1984	2.45, 2.09, 1.40		
1985	3.10, 2.34, 1.47		
1986	3.74, 2.54, 1.53		
1987		1.06, 1.07, 1.04	
1988		1.21, 1.22, 1.12	
1989		1.42, 1.41, 1.22	
1990		1.69, 1.61, 1.33	
1991		1.93, 1.77, 1.42	1.03, 1.04, 1.02
1992			1.26, 1.26, 1.11
1993			1.46, 1.42, 1.19
1994			1.71, 1.60, 1.27
1995			1.94, 1.74, 1.33
1996			2.12, 1.84, 1.37
1997			2.31, 1.93, 1.41
1998			2.51, 2.03, 1.46
1999			2.59, 2.06, 1.47
2000			2.59, 2.06, 1.47

Table 4. Tabulated α-Factors for the 0° Proton Channel of NOAA-15, 16, 17, 18 and METOP-02 for Mid Point (2 July) of Each Year[a]

Year	NOAA-15	NOAA-16	NOAA-17	NOAA-18	METOP-02
1998	1.00, 1.00, 1.00				
1999	1.01, 1.12, 1.08				
2000	1.06, 1.25, 1.17				
2001	1.13, 1.37, 1.25	1.09, 1.09, 1.07			
2002	1.39, 1.50, 1.33	1.24, 1.29, 1.21			
2003	1.64, 1.62, 1.41	1.37, 1.48, 1.36	1.20, 1.11, 1.12		
2004	1.86, 1.75, 1.50	1.46, 1.63, 1.50	1.36, 1.23, 1.25		
2005	2.03, 1.87, 1.58	1.52, 1.73, 1.64	1.46, 1.34, 1.37	1.00, 1.00, 1.00	
2006	2.13, 2.00, 1.66	1.53, 1.75, 1.79	1.51, 1.46, 1.50	1.00, 1.05, 1.03	
2007	2.16, 2.12, 1.73	1.53, 1.75, 1.81	1.52, 1.52, 1.56	1.00, 1.10, 1.06	1.05, 1.04, 1.03
2008	2.16, 2.24, 1.73	1.53, 1.75, 1.81	1.52, 1.52, 1.56	1.01, 1.14, 1.08	1.14, 1.10, 1.08
2009	2.16, 2.34, 1.73	1.53, 1.75, 1.81	1.52, 1.52, 1.56	1.01, 1.17, 1.11	1.20, 1.15, 1.13
2010	2.16, 2.34, 1.73	1.53, 1.75, 1.81	1.52, 1.52, 1.56	1.01, 1.17, 1.14	1.20, 1.15, 1.13
2011	2.16, 2.34, 1.73	1.53, 1.75, 1.81	1.52, 1.52, 1.56	1.01, 1.17, 1.17	1.20, 1.15, 1.13

[a]Each column contains the α-factors for the three lowest energy channels respectively (α_1, α_2, α_3). Note that at the launch of a satellite the α-factors are 1.0 for the given satellite.

in NOAA-10 measurements between 29.2.1988–30.9.1988. Figure 13 shows the ratio of corrected and uncorrected fluxes as a function of time for 90° telescope (Figure 13, top) and 0° telescope (Figure 13, bottom). The red curves depict the ratios corresponding to the revised correction and the cyan curves correspond to the corrected fluxes presented in AM2011. The dashed vertical lines in Figure 13 indicate launches of the NOAA satellites. One can see from Figures 12 and 13 that the uncorrected fluxes are nearly always much lower than the corrected fluxes. The uncorrected fluxes are close to the corrected fluxes only during rather short times after the launch when a single, still undegraded satellite is operational. Such times are in the beginning of NOAA-06, NOAA-10, NOAA-12 and NOAA-15 measurements in 1979, 1986, 1991 and 1998 respectively. Note that since no correction is applied to the NOAA-08 data the uncorrected and corrected fluxes are identical during those times when NOAA-08 is operational (see NOAA-08 era in Figure 14 when no other satellites are operational simultaneously with NOAA-08). At other times the MEPED instruments on operational NOAA satellites are significantly degraded and the proton fluxes are underestimated. The underestimation becomes severe already 1–2 years after satellite launch. As shown in Figure 13, the largest underestimation occurs near the end of NOAA-06 measurements in 1986 when the 90° fluxes are underestimated by over an order of magnitude and in 1997–1998 when the uncorrected 0° fluxes are roughly 13 times lower than the corrected ones. During the SEM-2 era starting at NOAA-15 launch in 1998 the uncorrected fluxes are on average about 2–3 times smaller than the corrected fluxes.

[27] Figures 12 and 13 also show the difference between the new revised correction and the correction presented in AM2011. During the SEM-2 era the differences between the old and the new correction are small. During this time the main difference between the two correction methods is the slightly different temporal evolution of some of the α factors (mainly in P3 channels) of some satellites. In contrast, for the SEM-1 satellites the two correction methods produce significantly different time series. To highlight the differences in the uncorrected and corrected SEM-1 time series and the differences between the two correction methods, Figure 14 shows the time series of each SEM-1 satellite separately, separated by the black vertical lines in the panels. The gray curves depict the uncorrected fluxes, the cyan curves the fluxes corrected according to AM2011 and the red curves depict the fluxes corresponding to the revised correction. Figure 14 shows that the most notable difference between the

Table 5. Same as Table 4 but for the 90° Telescope

Year	NOAA-15	NOAA-16	NOAA-17	NOAA-18	METOP-02
1998	1.00, 1.00, 1.00				
1999	1.08, 1.21, 1.12				
2000	1.20, 1.41, 1.23				
2001	1.35, 1.60, 1.33	1.03, 1.11, 1.06			
2002	1.56, 1.77, 1.38	1.14, 1.35, 1.17			
2003	1.81, 1.93, 1.49	1.31, 1.58, 1.29	1.28, 1.18, 1.11		
2004	2.12, 2.08, 1.68	1.50, 1.77, 1.40	1.50, 1.37, 1.21		
2005	2.40, 2.21, 1.88	1.68, 1.92, 1.52	1.65, 1.56, 1.32	1.00, 1.00, 1.00	
2006	2.56, 2.32, 1.92	1.83, 2.02, 1.64	1.72, 1.75, 1.43	1.02, 1.07, 1.05	
2007	2.69, 2.43, 1.92	1.88, 2.04, 1.70	1.73, 1.84, 1.49	1.05, 1.14, 1.09	1.05, 1.07, 1.03
2008	2.84, 2.52, 1.92	1.88, 2.04, 1.70	1.73, 1.84, 1.49	1.07, 1.20, 1.14	1.13, 1.19, 1.09
2009	2.96, 2.58, 1.92	1.88, 2.04, 1.70	1.73, 1.84, 1.49	1.09, 1.25, 1.17	1.20, 1.28, 1.13
2010	2.96, 2.58, 1.92	1.88, 2.04, 1.70	1.73, 1.84, 1.49	1.09, 1.25, 1.17	1.20, 1.28, 1.13
2011	2.96, 2.58, 1.92	1.88, 2.04, 1.70	1.73, 1.84, 1.49	1.09, 1.25, 1.17	1.20, 1.28, 1.13

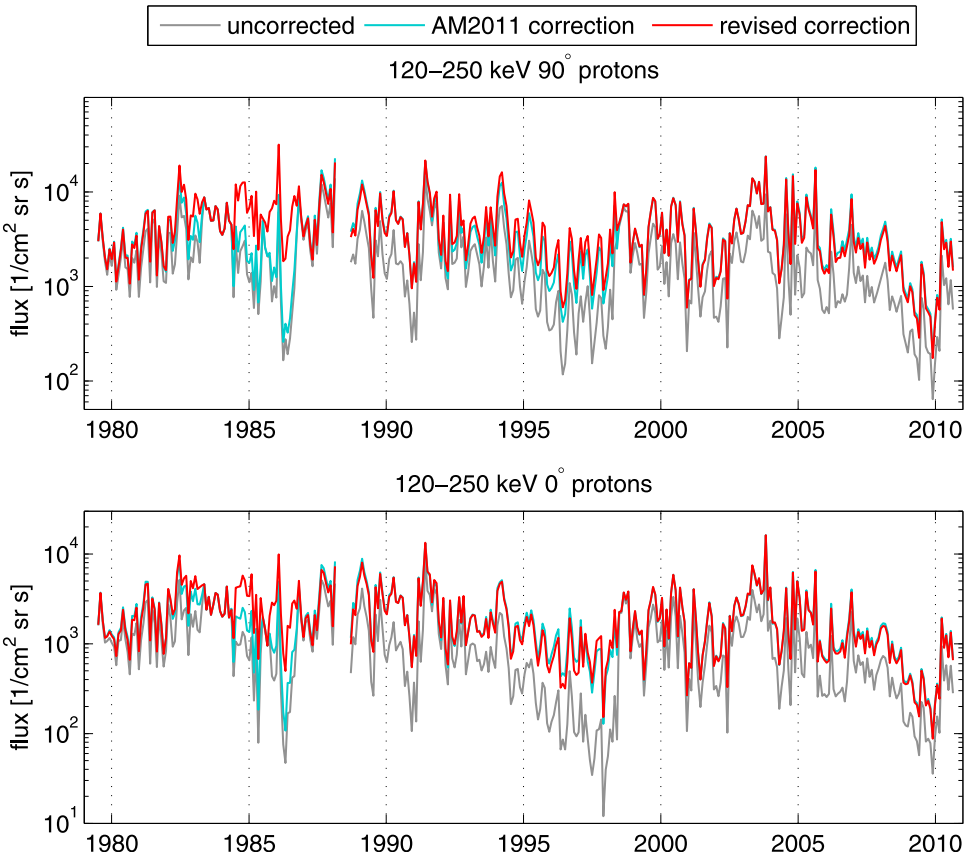

Figure 12. Overview of energetic proton measurements between 1979–2010. The panels show the 30-day averages of 120–250 keV protons from the (top) 90° and (bottom) 0° telescopes. The gray curves depict the uncorrected fluxes, the cyan curves the fluxes corrected according to AM2011 and the red curves the fluxes corresponding to the revised correction.

two correction methods exists in the NOAA-06 time series for which the older AM2011 correction method produces nearly an order of magnitude too low fluxes in 1985–1986. This difference is due to the serious underestimation of the NOAA-06 α factors in AM2011 (also seen in Figure 5). The new correction method raises the proton fluxes in 1985–1986 by nearly an order of magnitude from the corrected fluxes presented in AM2011, and connects the NOAA-06 time series smoothly to the NOAA-10 time series beginning in October 1986. For the NOAA-10 measurements the two correction methods do not differ significantly. The largest differences in 1987–1989 (barely visible in Figure 14) are due to the different temporal evolution of the α factors in AM2011 and here. In the NOAA-12 measurements the 90° fluxes show significant differences between the two correction methods. Generally, the revised correction produces slightly higher fluxes due to the revised α factors being slightly larger than in AM2011. In the 0° fluxes from 1991 to 1998 one can, perhaps surprisingly, see only a small difference between the two correction methods. The revised 0° α factors for NOAA-12 are significantly lower than in AM2011 due to the noise correction of the 0° fluxes introduced here. The noise correction has the effect of increasing the fluxes after mid 1996 while the lower α factors (compared to AM2011) tend to effectively decrease the fluxes. It appears that these two effects mostly compensate each other so that in the end the 0° fluxes produced by the two correction methods are quite similar.

10. Summary and Conclusions

[28] Here we have further studied the recently recalibrated energetic proton dataset provided by the NOAA/MEPED instruments. We pointed out and presented solutions to some newly found problems in the NOAA/MEPED instruments and the related energetic particle dataset. The implied modifications to the recalibrated dataset were evaluated and adopted. We showed that, besides degrading due to radiation damage, the NOAA-12 and NOAA-08 satellites suffer from effects of increased electronic noise in the back detector of the proton instrument. Increased back detector noise counts erase real counts from the front detector which measures the lower energy protons and leads to decrease in the fluxes at these energy channels. We showed how to correct this effect by modifying the baseline of the 0°/90° proton flux ratio. In our earlier work in AM2011 the statistical significance of the effective energy thresholds (α factors) of the older SEM-1 satellites was poor. Here we used daily averaged fluxes to obtain more robust estimates for the corrected energy thresholds. We also showed that the energy thresholds

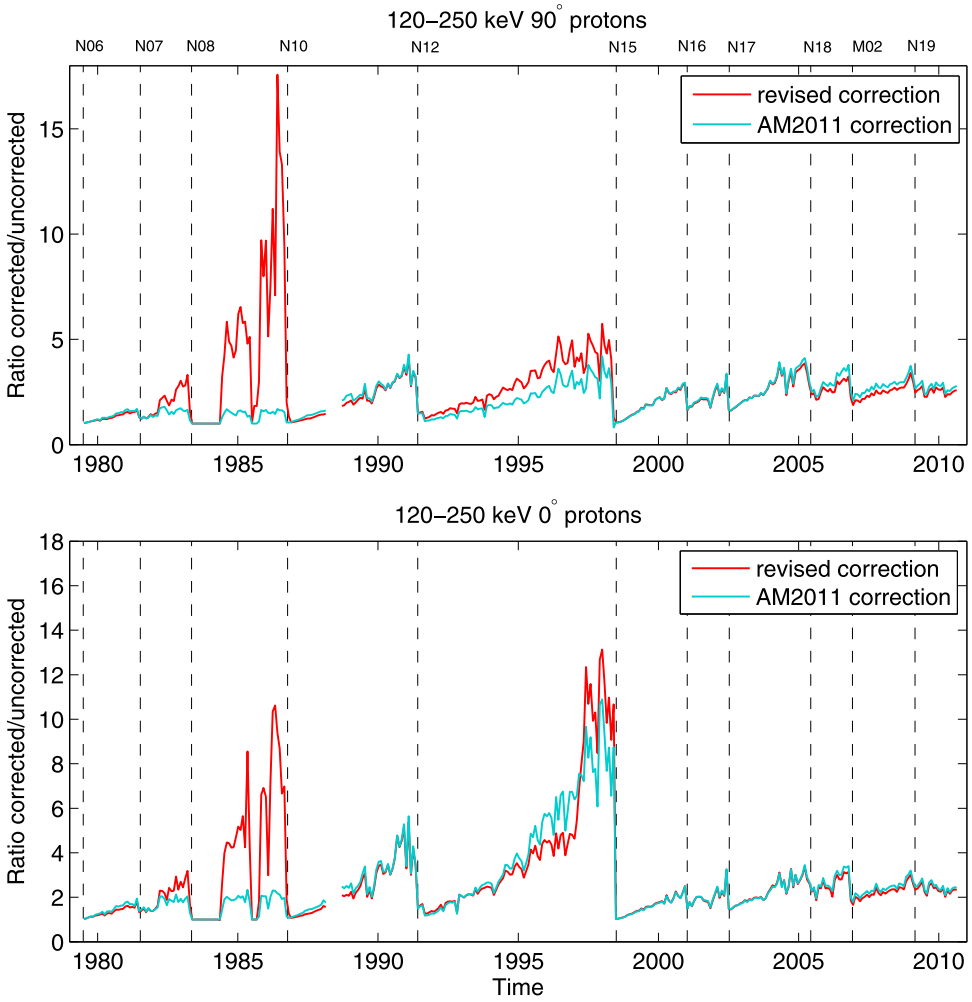

Figure 13. Ratio of corrected and uncorrected fluxes as a function of time for (top) 90° telescope and (bottom) 0° telescope. The red curves depict the ratios corresponding to the revised correction and the cyan curves correspond to the corrected fluxes presented in AM2011. The dashed vertical lines indicate launches of the NOAA satellites.

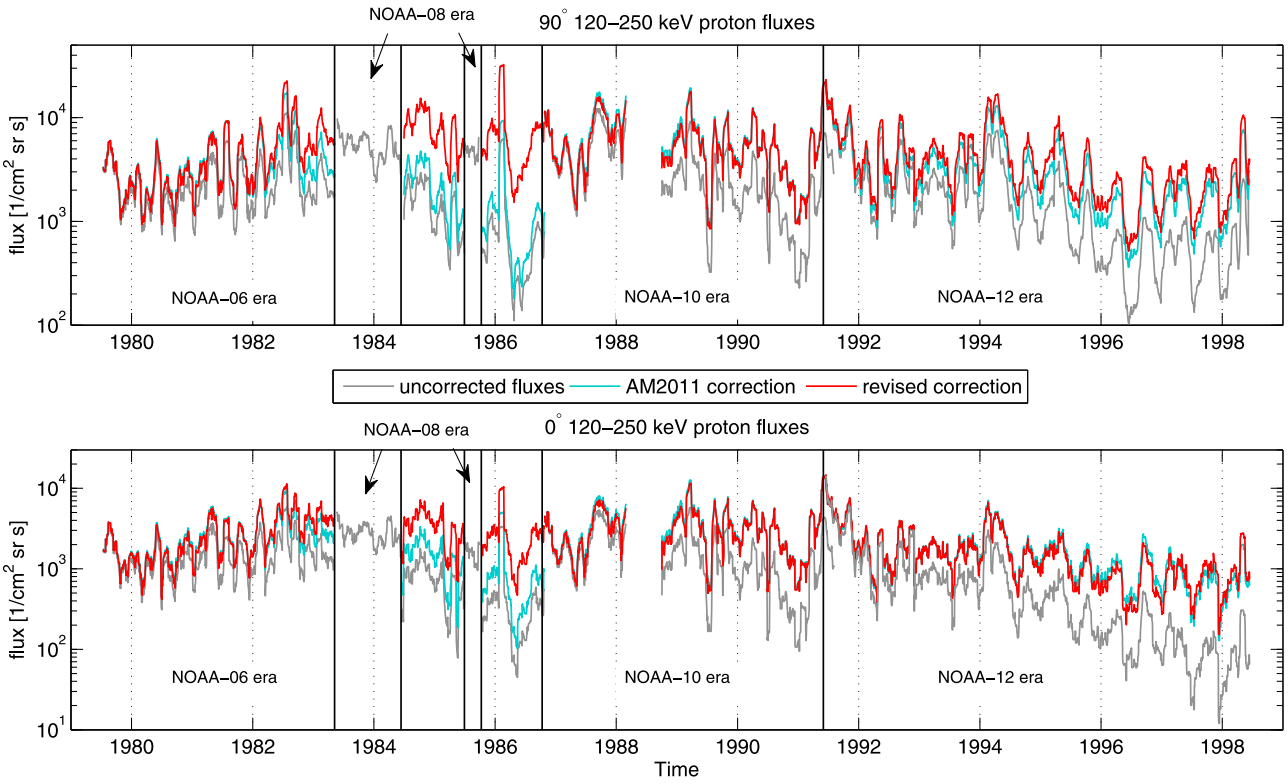

Figure 14. Overview of energetic proton measurements from the SEM-1 instruments between 1979–1998. The panels show the 30-day running averages of 120–250 keV protons from the (top) 90° and (bottom) 0° telescopes. The gray curves depict the uncorrected fluxes, the cyan curves the fluxes corrected according to AM2011 and the red curves depict the fluxes corresponding to the revised correction. The black vertical lines separate the time series of NOAA-06, NOAA-10 and NOAA-12 as indicated in the panels.

increase systematically with the cumulative Ap index computed separately for each satellite from its launch. Using this relation we could produce a more refined estimate for the temporal evolution of the energy thresholds.

[29] Using the above methods we computed the corrected MEPED energetic proton fluxes from 1979 to present. Using these fluxes we showed that the effective energy thresholds of all MEPED instruments increase systematically not only with the cumulative Ap index but with the cumulative particle fluxes observed by the instruments. Furthermore, this increase was observed to be similar in all satellites, thus proving that the energetic particles measured by the instruments are the cause for the radiation damage. We also compared the fluxes produced by the new correction methods presented here to the uncorrected fluxes and to the corrected fluxes presented earlier in AM2011. Overall we find that due to the effects of the radiation damage and the noise problem the fluxes can be underestimated by over an order of magnitude, and that this underestimation becomes severe already 1–2 years after the satellite launch. Comparing the new correction method to the earlier one we find that the new correction method mainly changes the fluxes of the older NOAA-06, NOAA-08, NOAA-10 and NOAA-12 satellites. The improvements in these satellites are introduced by the correction of the back detector noise and the improved estimates about the effective energy thresholds. In the most dramatic case in 1985–1986 the new correction raises the fluxes by nearly an order of magnitude from the earlier estimate and brings them to the correct level. Accordingly, the new corrections are essential to the long term homogeneity of the whole NOAA/MEPED data series, which now forms the longest systematically calibrated energetic particle dataset in space physics, covering almost continuously three solar cycles from 1979 to present.

[30] **Acknowledgments.** We greatly acknowledge the help provided by Dave Evans in analyzing the MEPED data. The data presented in Figure 2 was originally computed by Robert Bushnell and kindly provided by Dave Evans. We acknowledge the support by the Academy of Finland to the post doctoral project of T. Asikainen (134547) and to the HISSI research project 128189, by the Thule Institute of University of Oulu, and by the Emil Aaltonen Foundation. We gratefully acknowledge support for this work via the Near-Earth Space Data Infrastructure for e-Science project (www.espas-fp7.eu), which is funded by the Research Infrastructures theme of the EU Framework 7 programme under grant agreement 283676.

References

Asikainen, T., and K. Mursula (2005), Filling of the South Atlantic Anomaly by energetic electrons during a great magnetic storm, *Geophys. Res. Lett.*, *32*, L16102, doi:10.1029/2005GL023634.

Asikainen, T., and K. Mursula (2008), Energetic electron flux behavior at low L-shells and its relation to the South Atlantic Anomaly, *J. Atmos. Sol. Terr. Phys.*, *70*, 532–538.

Asikainen, T., and K. Mursula (2011), Recalibration of NOAA/MEPED energetic proton measurements, *J. Atmos. Sol. Terr. Phys.*, *73*, 335–347, doi:10.1016/j.jastp.2009.12.011.

Asikainen, T., R. Kerttula, K. Mursula, R. Friedel, D. Baker, F. Søraas, J. Fennell, and J. Blake (2005), Global view of energetic particles during

a major magnetic storm, in *The Inner Magnetosphere: Physics and Modeling*, *Geophys. Monogr. Ser.*, vol. 155, edited by T. Pulkkinen, N. Tsyganenko, and R. Friedel, pp. 97–104, AGU, Washington, D. C.

Asikainen, T., V. Maliniemi, and K. Mursula (2010), Modeling the contributions of ring, tail and magnetopause currents to the corrected Dst index, *J. Geophys. Res.*, *115*, A12203, doi:10.1029/2010JA015774.

Evans, D. S., and M. S. Greer (2000), Polar orbiting environmental satellite space environment monitor—2: Instrument descriptions and archive data documentation, *NOAA Tech. Memo., OAR SEC-93*, NOAA, Boulder, Colo.

Evans, D., H. Garrett, I. Jun, R. Evans, and J. Chow (2007), Long-term observations of the trapped high-energy proton population (L < 4) by the NOAA Polar Orbiting Environmental Satellites (POES), *Adv. Space Res.*, *41*(8), 1261–1268, doi:10.1016/j.asr.2007.11.028.

Fung, S. (1996), Recent development in the NASA trapped radiation models, in *Radiation Belts: Models and Standards*, *Geophys. Monogr. Ser.*, vol. 97, edited by J. Lemaire, D. Heynderickx, and D. Baker, pp. 79–91, AGU, Washington, D. C.

Fung, S., X. Shao, and L. Tan (2006), Long-term variations of the electron slot region and global radiation belt structure, *Geophys. Res. Lett.*, *33*, L04105, doi:10.1029/2005GL024891.

Galand, M., and D. Evans (2000), Radiation damage of the proton MEPED detector on POES (TIROS/NOAA) satellites, *NOAA Tech. Memo., OAR 456-SEC 42*, NOAA, Boulder, Colo.

Grupen, C., and B. Shwartz (2008), *Particle Detectors*, *Cambridge Monogr. on Part. Phys., Nucl. Phys. and Cosmol.*, vol. 26, 2nd ed., Cambridge Univ. Press, Cambridge, U. K.

Hill, V. J., D. S. Evans, and H. H. Sauer (1985), TIROS-N/NOAA satellites Space Environment Monitor archive tape documentation, *NOAA Tech. Memo., ERL SEL-71*, NOAA, Boulder, Colo.

Huston, S., G. Kuck, and K. Pfitzer (1996), Low altitude trapped radiation model using TIROS/NOAA data, in *Radiation Belts: Models and Standards*, *Geophys. Monogr. Ser.*, vol. 97, edited by J. Lemaire, D. Heynderickx, and D. Baker, pp. 119–122, AGU, Washington, D. C.

Lam, M., R. Horne, N. Meredith, S. Glauert, T. Moffat-Griffin, and J. Green (2010), Origin of energetic electron precipitation >30 keV into the atmosphere, *J. Geophys. Res.*, *115*, A00F08, doi:10.1029/2009JA014619.

Lutz, G. (1999), *Semiconductor Radiation Detectors*, 1st ed., Springer, Berlin.

McFadden, J., et al. (2007), In-flight instrument calibration and performance verification, in *Calibration of Particle Instruments in Space Physics*, *ISSI Sci. Rep.*, vol. SR-007, edited by M. Wüest, D. S. Evans, and R. von Steiger, pp. 277–385, Eur. Space Agency, Paris.

Raben, V. J., D. S. Evans, H. H. Sauer, S. R. Sahm, and M. Huynh (1995), TIROS/NOAA satellite Space Environment Monitor data archive documentation: 1995 update, *NOAA Tech. Memo., ERL SEL-86*, NOAA, Boulder, Colo.

Rodger, C., M. Clilverd, J. Green, and M. Lam (2010), Use of POES SEM-2 observations to examine radiation belt dynamics and energetic electron precipitation into the atmosphere, *J. Geophys. Res.*, *115*, A04202, doi:10.1029/2008JA014023.

Seale, R. A., and R. H. Bushnell (1987), The TIROS-N/NOAA A-J Space Environment Monitor subsystem, *NOAA Tech. Memo., ERL SEL-75*, NOAA, Boulder, Colo.

Søraas, F., K. Aarsnes, and K. Oksavik (2002), Ring current intensity estimated from low-altitude proton observations, *J. Geophys. Res.*, *107*(A7), 1149, doi:10.1029/2001JA000123.

Søraas, F., K. Aarsnes, K. Oksavik, M. Sandanger, D. Evans, and M. Greer (2004), Evidence for particle injection as the cause of Dst reduction during HILDCAA events, *J. Atmos. Sol. Terr. Phys.*, *66*, 177–186.

Wissing, J., J. Bornebusch, and M.-B. Kallenrode (2008), Variation of energetic particle precipitation with local magnetic time, *Adv. Space Res.*, *41*, 1274–1278.

Yando, K., R. Millan, J. Green, and D. Evans (2011), A Monte Carlo simulation of the NOAA POES Medium Energy Proton and Electron Detector instrument, *J. Geophys. Res.*, *116*, A10231, doi:10.1029/2011JA016671.